

A General Free Wake Geometry Calculation For Wings and Rotors

Wayne Johnson

*Johnson Aeronautics
Palo Alto, California*

A general free wake geometry calculation for wings and rotors is presented. The method, which has been implemented in CAMRAD II, gives good performance and airloads correlation at advance ratios of 0.05 and above, with reasonable computation speed. The wake geometry distortion can be calculated for multiple wings, multiple rotors, and non-identical blades; for all wake structures, including multiple rolled-up trailed vorticity and inboard sheets as well as tip vortices; using the same wake model as the induced velocity calculations; for transients as well as the trim solution. The theoretical approach is described. Results are presented for rotor airloads, flapping, and performance, including comparisons with a common wake geometry method and with measured data. Calculated wake geometries are shown for a nonrotating wing, a single rotor, multiple main rotors, and a wind turbine.

Notation

C	influence coefficient
C_T	rotor thrust coefficient, $T/\rho\pi R^2(\Omega R)^2$
D	wake self-induced distortion
G	wake vorticity strength
q	induced velocity at point on wake
R	rotor radius
r_Q	wing position
r_W	wake geometry
t	time
V	rotor speed relative air
v_W	wind velocity
α_s	rotor shaft angle of attack (+ rearward)
α_{tpp}	tip-path-plane angle of attack (+ forward)
Γ	wing bound circulation
δ	time wake vorticity element created, $t-\tau$
μ	advance ratio, $V/\Omega R$
ρ	air density
σ	rotor solidity ratio (ratio blade area to disk area)
τ	wake age
Ω	rotor rotational speed

Introduction

The rotor vortex wake is an important factor in most problems of helicopters, including poor performance, high blade loads, high vibration, and high noise levels. An accurate calculation of the wake-induced nonuniform inflow and the resulting blade airloads is needed in order to predict rotor behavior. Below an advance ratio of about $\mu = 0.20$, blade-vortex interaction is particularly strong and therefore an accurate wake geometry is needed as well.

The task of calculating rotor aerodynamics can be divided into steps, as shown in figure 1. First the wake geometry must be calculated, then the influence coefficients and induced velocity calculated, and finally the coupled aerodynamics and dynamics of the rotor solved. Typically an iterative procedure is required, since the blade motion and bound circulation influence the wake geometry and wake calculations. This division is also reflected in the implementation of the calculations, which can use separate models for the wake geometry, the wake, and the wing. The subject of this paper is the wake geometry model. A general free wake geometry calculation for wings and rotors is presented. The theoretical basis of the wake geometry calculation is described, and results are presented for rotor wake geometry, airloads, flapping, and performance. Correlation with measured airloads, flapping, and performance is shown.

*Presented at the American Helicopter Society 51st Annual Forum, Fort Worth, Texas, May 9–11, 1995.
Copyright © 1995 Wayne Johnson. All rights reserved.*

Table 1 summarizes the wake geometry and wake models used in several rotorcraft analyses. These wake models were all developed by Johnson (refs. 1–7). The Scully wake geometry model is described in reference 15 (that reference also develops a model for the wake and wing calculations, which is not however used in any of the analyses listed in table 1). The Johnson wake geometry model and the general wake geometry model are described in full in reference 7; these models are the subject of this paper. The wake geometry calculation method labeled "Scully" (ref. 15) is currently used in many rotorcraft analyses (table 1). This method has the following characteristics:

Advantages:

- a) good performance and airloads correlation at advance ratios $\mu = 0.125$ and above;
- b) fast operation.

Limitations:

- c) poor results at $\mu = 0.1$ and below;
- d) distorted geometry calculated for one rotor, identical blades, only tip vortex, single peak circulation distribution, only trim.

The wake geometry calculation method labeled "Johnson" was developed to provide good results at very low speeds, while retaining the capabilities of the Scully method. Its characteristics are:

Advantages:

- a) good performance and airloads correlation at advance ratios $\mu = 0.125$ and above;
- b) computation speed comparable to Scully method;
- c) good results at $\mu = 0.1$ and below.

Limitations:

- d) distorted geometry calculated for one rotor, identical blades, only tip vortex, single peak circulation distribution, only trim.

The wake geometry method labeled "general" was developed for CAMRAD II, using the same approach as the Johnson method. Its characteristics are:

- a) distortion calculated for multiple wings, multiple rotors, non-identical blades;
- b) distortion calculated for all wake structures, including multiple rolled-up trailed vorticity and inboard sheets as well as tip vortices;
- c) same wake model as wake calculations (influence coefficient and induced velocity calculations);
- d) transient as well as trim.

The Scully, Johnson, and general free wake geometry methods are compared in this paper.

Background

The wake geometry describes the position of the wake vorticity in space. The undistorted geometry is obtained from the motion of the wing: a wake element is convected by the wind, from the position in the air at which it was created. This geometry is distorted by the wake self-induced velocity. A rigid wake geometry is obtained by assuming that the wake elements are all convected by the average interference velocity at the wings. A free wake geometry is obtained by calculating the distortion simultaneously for all wings.

The free distortion is calculated by integrating in time the self-induced velocities at all collocation points on all wakes of the wings. Special techniques are required to keep the computational effort reasonable. The following are the key aspects of the approach, both from previous work and as developed for the present work.

- a) When calculating the velocity at a collocation point, the wake is divided into "near wake" and "far wake" regions. The velocity contribution of the far wake is small, so when the velocity is required again in the algorithm, only the contribution of the near wake need be recalculated (ref. 16).
- b) The near wake regions are defined by transition points between far wake and near wake. It is assumed that the relative age of these transition points depends on the time the wake element was created, but not on the wake age (ref. 15).
- c) During the basic time step, the existing wake is convected by the wind and the induced velocity with little relative distortion, while the wings move and generate new wake behind the trailing edges (ref. 15).
- d) Trapezoidal integration is used for stability, but the primary contribution to the velocity is only calculated once for a time step (ref. 15).
- e) Integration of the wing-induced velocity in time is approximately equal to the average velocity from the bound vortex (a vortex line segment), which is equivalent to the velocity from a vortex sheet element (ref. 15).
- f) The effect of the core vorticity distribution on the self-induced velocity of a vortex arc is obtained using an appropriate cutoff distance (ref. 17).
- g) The wake model of the wing wake calculation (influence coefficient and induced velocity calculations) is used for the free distortion calculation, including features such as the dual-peak model; multiple rollup of the trailed vorticity; and models for entrainment and stretching in the rollup process.

h) The calculation of the distortion is performed with time as the outer loop, for both trim and transient tasks. The trim distortion is constant or periodic (in an appropriate frame). The calculation includes an iteration between revolutions with velocity relaxation and propagation; and an outer iteration with distortion relation.

i) The velocity at a collocation point is calculated with a full update (including determination of the near wake regions), a near wake update, or no update. The update frequency can be chosen to balance efficiency and accuracy. The velocity can be updated more often for collocation points with small wake age (young wake), to improve accuracy of the geometry up to an interaction with a following wing.

j) In the trapezoidal integration, the primary contribution to the velocity is calculated at the beginning of the time step.

The calculation method is described in more detail by the following sections.

Distortion Calculation

The undistorted geometry is calculated from the position in the air at which the wake element was created, plus convection by the wind. Then the distortion produced by the self-induced velocities of the rotor is added. Let t be the current time, and τ the age of the element in the wake. Thus $\delta = t - \tau$ is the time when the vorticity was created. Then

$$r_W(t, \tau) = r_Q(t - \tau) + \tau v_W + D(t, \tau)$$

is the wake geometry. Here v_W is the constant wind velocity; and r_Q is the wing position, evaluated at past times. Note that the time at which the vorticity was created ($t - \tau$) identifies a particular element in the wake. The wake geometry distortion $D(t, \tau)$ is the perturbation of the position from the undistorted geometry, in inertial axes. By definition the wake geometry connects to the wing at $\tau = 0$, so $D(t, 0) = 0$. The distortion is produced by the self-induced velocities in the rotor. The free distortion is calculated for wake ages up to τ_{\max} .

The wake geometry is calculated for a set of wings undergoing arbitrary motion through the air. This set of wings can be nonrotating, a rotor, or several rotors. In the following description, the term "rotor" refers to all the wings in the set. The wake trailed vorticity can be divided into several spanwise panels. The wake geometry is described by the positions of the vortex elements at the boundaries of these panels, separately for the tip vortices and the inboard sheet edges if the trailed wake rolls up at a boundary. The wake geometry distortion can be calculated optionally for the tip vortices; for all the rolled-up trailed

vortices; and for the inboard sheet edges as well. The rigid distortion is used where the free distortion is not calculated. The possibility that the distortion is identical for different wings (perhaps with a time shift) is not considered in the general method. The distortion is required for all structures of the wake geometry: for the left and right tip vortices, and the left and right edges of the inboard sheet; for each trailed wake panel; for each wing. The distortion is initialized to the rigid geometry for all structures: $D(t, \tau) = v_{\text{conv}}\tau$, where v_{conv} is the mean convection velocity of the wake. Thus the rigid distortion is used where the free distortion is not calculated.

The distortion may be required at an age τ beyond which it has been calculated. Let τ_{last} be the maximum age of the available distortion. The distortion is extrapolated by assuming that the vortex element is convected for time $(\tau - \tau_{\text{last}})$ by a constant velocity:

$$D(t, \tau) = D(t - (\tau - \tau_{\text{last}}), \tau_{\text{last}}) + (\tau - \tau_{\text{last}})v_{\text{conv}}$$

Note that the distortion is used at a constant value of δ . The distortion is calculated and used in the inertial frame. For the trim task, it is assumed that the wake geometry distortion is constant or periodic, in an appropriate frame. The trim distortion is calculated over a reference revolution t_Z to $t_Z + T$, where T is the period, and the start of the revolution t_Z is defined by the solution procedure.

The distortion is calculated by integrating in time the self-induced velocity q acting on the wake element created at time $\delta = t - \tau$:

$$D(t, \tau) = \int_{t-\tau}^t q(t = \sigma, \tau = \sigma - \delta) d\sigma$$

The integration is performed for fixed δ . The velocity q does not include the wind velocity. The induced velocity is evaluated by integrating over all vorticity in the wake. For incompressible flow, the Biot-Savart law gives the velocity as an integral of the wake strength times an influence coefficient:

$$q(t) = \iint C(t, \tau, r) G(t, \tau, r) dr d\tau$$

here τ is the wake age and r the wing span variable, so the integral is over the wake surface. The influence coefficient C depends on the wake geometry. The wake strength G depends on the wing bound circulation at past times, $\Gamma(t - \tau, r)$.

The wake age is discretized by using the geometry and strength only at a set of ages $\tau_k = k\Delta\tau$, $k = 0$ to K , for fixed wake age increment $\Delta\tau$. Time is discretized in the distortion calculation, with fixed increment Δt . The time increment and the wake age increment must be equal, $\Delta t = \Delta\tau$, in order to implement the integration algorithm.

The number of steps J in one revolution is defined. Then if the trim distortion is periodic, the time increment $\Delta t = T/J$ is calculated from the period T . If the trim distortion is constant, Δt must be specified directly. The distortion calculation in the transient task uses the time increment from the trim task.

For the trim task, the distortion is calculated over one revolution: $t = t_Z$ to $t = t_Z + J\Delta t = t_Z + T$. The start of the revolution t_Z is defined by the solution procedure. At the first time step of the solution procedure, the distortion is calculated for the entire rotor simultaneously, for the entire revolution, using the time increment Δt and wake age increment $\Delta\tau = \Delta t$ of the wake geometry analysis. Then from this saved distortion, the wake analysis evaluates as required the wake geometry for one wing; interpolated or extrapolated to the times of the solution procedure, and the wake ages of the wake analysis.

For the transient task, the distortion is calculated over the time range t_B to $t_E = t_B + N\Delta t$, where t_B and t_E are defined by the solution procedure. The transient distortion is initialized at t_B using the trim distortion at $t_B = t_Z + j_B\Delta t$ (which need not be in the trim reference revolution). At each step of the solution procedure, the distortion is calculated for the entire rotor simultaneously, for times from $t_B + j\Delta t$ up to the current time, using the time and wake age increment Δt of the wake geometry analysis. Then from this saved distortion, the analysis evaluates as required the wake geometry for one wing; interpolated or extrapolated to the times of the solution procedure, and the wake ages of the wake analysis.

Since the trim distortion is periodic or constant, the solution process includes an outer iteration. This is a successive substitution iteration, with relaxation on the distortion to improve convergence. A specified number of iterations are performed; there is no test for convergence. Often relaxation is not required, and with the relaxation factor $\lambda_I = 1$ the iteration is equivalent to simply extending the time integration more revolutions. Hence the iteration can be omitted. The basic loop of the process is the integration in time, which is performed for M revolutions, each revolution covering the period T . The trim distortion is stored only for the reference revolution. The number of revolutions in the time integration should be greater than the maximum wake age, so the new wake generated is at least equal to the amount of distortion needed. Typically $MT = 2\tau_{\max}$ is used. For each time step, the velocity q at a collocation point is integrated to get the change in distortion there, during time $t-\Delta t$ to t . At time t , the wake strength and distortion are known at $t-\Delta t$, so the velocity at $t-\Delta t$ can be calculated. During the trim task, the wake strength is known at t (since the circulation is periodic), but only an estimate of the distortion is available at t . During the transient task, the

wake strength and distortion are not yet calculated at t , unless the transient solution procedure includes wake and circulation loops.

The distortion is calculated by integrating the self-induced velocity q acting on the wake element created at time δ . The discretized integral at time t for $\delta = t-\Delta t-\tau$ is:

$$D(t, \tau+\Delta t) = D(t-\Delta t, \tau) + \int_{t-\Delta t}^t q(t=\sigma, \tau=\sigma-\delta) d\sigma \\ = D(t-\Delta t, \tau) + \Delta D$$

Numerical integration gives

$$\text{Euler: } \Delta D = q(t-\Delta t, \tau) \Delta t$$

$$\text{trapezoidal: } \Delta D = \frac{1}{2} (q(t, \tau+\Delta t) + q(t-\Delta t, \tau)) \Delta t$$

The trapezoidal method is used, since this Euler method is only conditionally stable. However, the trapezoidal method requires that the velocity be calculated twice per step, and the solution is not yet known at time t . Thus the following approximation is made. The relative distortion of the wake from $t-\Delta t$ to t is ignored, so during this time the only change is the addition of new wake of age $\tau = 0$ to Δt directly behind the wings. Then excluding the velocity from the bound vortices:

$$q(t, \tau+\Delta t) \approx q(t-\Delta t, \tau) + q_1(\tau)$$

where q_1 is the velocity at t of the new wake generated behind the wing during $t-\Delta t$ to t . Thus the integral becomes:

$$D(t, \tau+\Delta t) = D(t-\Delta t, \tau) \\ + [q_T(\tau) + \frac{1}{2} q_1(\tau) + q_B(\tau)] \Delta t \\ = D(t-\Delta t, \tau) + q \Delta t$$

where q_T is the total velocity (excluding the bound vortices) at time $t-\Delta t$, and q_B is the effect of the wing-induced velocities (bound vortices). It is necessary to keep q_B separate since the wing vorticity moves with the wing rather than being convected with the fluid. Note that reference 15 uses

$$q(t-\Delta t, \tau) \approx q(t, \tau+\Delta t) - q_1(\tau)$$

instead. Since the velocity and distortion are periodic in time, relaxation of the velocity can be introduced to improve convergence. Both numerical and physical instabilities are possible in the free distortion calculation, so typically a relaxation factor of $\lambda_R = 0.5$ or less is needed. In addition, propagation of the distortion information can be included in the trim solution. The distortion increment $\Delta D = q\Delta t$ is not the same as that calculated during the last revolution; the difference is $\delta D = (q-q_{\text{old}})\Delta t$. The difference δD affects all future values

of D at this $\delta = t - \tau$. Since the trim distortion is periodic, δD also affects values of D at past times and larger age. Thus the propagation procedure adds δD to all values of $D(t, \tau)$ at future time t and fixed $t - \tau$ (subtracting the period T from t whenever the time exceeds the reference revolution, while τ is less than the maximum wake age τ_{\max}).

Velocity Calculation

The velocity contributions q_T , q_1 , and q_B are required at time $t - \Delta t$, for wake ages $\tau = 0$ to $\tau_{\max} - \Delta t$. These velocities are calculated at a collocation point that is on the wake (as specified by the wake structure and age). As defined above, q_T is the total wake-induced velocity (excluding the bound vortices) at time $t - \Delta t$; q_1 is the velocity at t of the new wake generated behind the wing during $t - \Delta t$ to t ; and q_B is the effect of the wing-induced velocities (bound vortices) during $t - \Delta t$ to t . In order to minimize the computational effort in calculating q_T , for each collocation point the wake is divided into "near wake" and "far wake" regions. The velocity contribution of the far wake is small, so when the velocity is required again in the algorithm, only the contribution of the near wake need be recalculated. Thus the following update strategy is used in calculating q_T .

- Full update every n_F steps in time t : Calculate q_T by summing the velocity contributions from all elements in the wake. The near wake and far wake regions are determined, in terms of the wake age relative the collocation point. The wake of age τ_{le} (at the element leading edge) behind the i -th wing is in the near wake if $|\Delta q| > \Delta q_{NW}$, where Δq_{NW} is an input criterion and Δq is the sum of the velocities from all vortex elements at τ_{le} . The contribution to q_T from the far wake is stored as q_{far} .
- Else near wake update every n_N steps in time t : Calculate q_T by summing the velocity contributions from all elements in the near wake, and adding the contribution of the far wake, $q_T = q_N + q_{far}$.
- Else no update: Calculate q_T at time $t - \Delta t$ from the contribution of the new wake (created during last time step), and q_T at the previous time step, $q_T(t - \Delta t, \tau) = q_T(t - 2\Delta t, \tau - \Delta t) + q_1$.
- The velocity can be updated more often for collocation points with small wake age, to improve accuracy of the geometry up to an interaction with a following wing. Thus the young wake and elder wake, defined by age τ_{young} , can have different update frequencies and different near wake criteria.

The full and near wake update frequencies are chosen to balance efficiency and accuracy. During the basic time

step, the existing wake is convected by the wind and the induced velocity with little relative distortion, while the wings move and generate new wake behind the trailing edges. Thus with no update, only the velocity contribution from this new wake is calculated. As the wake distorts, it is necessary to recalculate the velocity from at least the near wake in order to maintain accurate integration. A full update involves the most computation, but also gives the most accurate value for the total velocity.

The near wake regions are defined by transition points between far wake and near wake. The near wake is determined during a full update calculation of the velocity for a collocation point at age τ on a wake structure; it consists of regions $\tau_{le} = \tau_{TB}$ to $\tau_{le} = \tau_{TE}$ behind the i -th wing. These transition points are used during a near wake update. In order to minimize storage, it is assumed that the relative age of these transition points (from $\tau_{TB} - \tau$ to $\tau_{TE} - \tau$) depends on the time the wake element was created, $\delta = t - \tau$, but not on the wake age τ . The near wake and far wake are defined by n_T sets of transition points τ_{TB} and τ_{TE} , and the velocity contribution q_{far} of the far wake. These quantities are stored as a function of $\delta = t - \tau$ (and wing number i for the transition points).

The wake model of the wing wake analysis is used for the free distortion calculation. In the rolled-up wake, the trailed vorticity can be divided into several spanwise panels. For each panel, the wake strength depends only on the peak bound circulation values (left and right peaks, or maximum). The self-induced velocity at a collocation point r_P must be evaluated at time t , from the wake geometry at t and the bound circulation at t and all past time. The wake is discretized in both span and age. Thus the integral equation for the wake-induced velocity becomes:

$$q(t) = \sum_{\text{wings}} \sum_{\text{panels}} \sum_{k=0}^{K_W} (C_L(t, \tau_k) G_L(t, \tau_k) + C_R(t, \tau_k) G_R(t, \tau_k))$$

including a summation over all wings of this analysis, and perhaps a summation over spanwise panels as well. The wake vorticity strength is $G(t, \tau) = \Gamma(t - \tau)$. For a single-peak circulation distribution, there is only one term, from either the maximum circulation or the outboard peak. The collocation point r_P is located at some age less than τ_{\max} on the wake. The wake used to calculate the induced velocity there extends from the wing to M_{below} revolutions below the collocation point ($k = 0$ to K_W).

The induced velocity is calculated as in the wing wake analysis. Since the collocation points are now on the

wake surface, special treatment is required for the induced velocity from vortex elements adjacent to the collocation point. For a collocation point on a rolled-up trailed vortex line, the induced velocity from the two adjacent line segments is calculated by replacing them by circular-arc vortex line segments. The effect of the core vorticity distribution on the self-induced velocity of a vortex arc is obtained using an appropriate cutoff distance (ref. 17). For a collocation point on an inboard vortex sheet, no change is considered appropriate for the typical case where the sheet is approximated by line segments with large cores. If vortex sheet elements are used, a large sheet thickness can be specified if necessary.

The term q_1 is the velocity at a collocation point for time t , from the new wake generated behind the wings during $t-\Delta t$ to t . During this time interval, the collocation point has been convected by the wind (changes in the distortion are being ignored for q_1). The relative geometry between the collocation point and the wake is thus unchanged if instead the collocation point remains at its position for time $t-\Delta t$, and the wake is convected by the negative wind. The position and strength of the new wake are then:

$$\text{leading edge: } r_W(t-\Delta t, \tau = -\Delta t) = r_Q(t) - \Delta t v_W \\ G(t-\Delta t, \tau = -\Delta t) = \Gamma(t)$$

$$\text{trailing edge: } r_W(t-\Delta t, \tau = 0) = r_Q(t-\Delta t) \\ G(t-\Delta t, \tau = 0) = \Gamma(t-\Delta t)$$

So the conventions of the analysis allow the position and strength of the new wake to be obtained at time $t-\Delta t$ with wake ages $\tau_{le} = -\Delta t$ and $\tau_{te} = 0$ (even though the wake does not actually exist for negative wake age).

The term $\Delta D = q_B \Delta t$ is the distortion produced by the wing-induced velocities (bound vortices) during $t-\Delta t$ to t . As in the calculation of the velocity from the new wake, the collocation point can remain at its position for time $t-\Delta t$, while instead the wake is convected by the negative wind. Integration of the wing-induced velocities during this time interval gives the distortion:

$$\Delta D = \int_{t-\Delta t}^t q_{\text{wing}} dt = q_B \Delta t$$

so q_B is the average wing-induced velocity. For an instantaneous value of the wing-induced velocity, a good model of the flow about the wing would be required. For the average value, representing the wing by a bound vortex appears to be adequate. The average velocity from the bound vortex (a line vortex) as the wing moves from time $t-\Delta t$ to time t is equivalent to the velocity produced by a vortex sheet defined by the wing positions. The bound vortex position and strength are the same as

required for the new wake position and strength (q_1). The strength of the vortex sheet should vary linearly from $\Gamma(t-\Delta t)$ at the trailing edge to $\Gamma(t)$ at the leading edge. The vortex sheet element being used assumes constant strength of the shed vorticity in this direction, so the element must have zero strength at the leading edge and strength

$$\frac{1}{2} (\Gamma(t) + \Gamma(t-\Delta t))$$

at the trailing edge. For efficiency, a rectangular-planar approximation of the wake sheet geometry is used; and the velocity is calculated from a line segment unless its magnitude is greater than an input criterion Δq_{BV} .

Parameters

The parameters of the wake model must be chosen to balance efficiency and accuracy. Table 2 summarizes the parameter values determined to give good results for rotor problems. Good performance and airloads results can be obtained with the "baseline" parameter values at advance ratios of 0.125 and above. Good performance results can be obtained with the "low speed" parameter values at advance ratios of 0.05 and above.

Applications and Correlation

Results are presented for rotor wake geometry, airloads, flapping, and performance, including correlation with measured data. The results are labeled "CAMRAD/JA" or "CAMRAD II":

CAMRAD/JA: Scully free wake geometry method (used in CAMRAD/JA, COPTER, RDYNE, UMARC, 2GCHAS, CAMRAD, CAMRAD II).

CAMRAD II: Johnson or general free wake geometry method.

All cases were actually run using CAMRAD II, so the same wake and wing models could be used (figure 1), and the only difference in the calculations is the wake geometry method. The first objective was to retain the capabilities of the Scully method, which will be demonstrated by considering airloads calculations at low speed. Then the improved capabilities of the general method will be demonstrated by considering lateral flapping and performance calculations.

The section lift on a rotor blade tip exhibits the influence of blade-vortex interaction at low speed. Figures 2 and 3 show the blade section lift calculated for the H-34 and SA-349/2 rotors. Table 3 summarizes the rotor parameters and operating conditions. The flight test results are from references 18 and 19. The CAMRAD/JA results were discussed in reference 20. Airloads for a section near the blade tip are shown in figures 2 and 3;

results at other radial stations are similar. A tip vortex core radius of 20% chord was used in the calculations. At these speeds, the CAMRAD/JA and CAMRAD II results are essentially the same. The nonuniform inflow model with free wake geometry is required in order to capture the strong blade-vortex interaction of low speed flight.

Table 4 compares the computation times of the two methods, for just the free distortion calculation. The CAMRAD II method with baseline parameters gives results comparable to the CAMRAD/JA method, for about four times the computational time. Considering the computation time for the entire job, this extra time is not important in CAMRAD/JA, and is not noticeable in CAMRAD II. Hence computational efficiency has been maintained. With the CAMRAD II free wake geometry method, the parameters can be adjusted for the problem to be solved, so good results can be obtained at low speed, at the cost of increased computation time.

Lateral flapping in low-speed forward flight is a sensitive measure of the effects of the rotor wake. Figure 4 shows the flapping and power for a model rotor. Table 3 summarizes the rotor parameters and operating conditions. The wind tunnel test results are from reference 21. The CAMRAD/JA results were discussed in reference 20. A tip vortex core radius of 20% chord was used in the calculations, with four revolutions of wake vorticity and wake geometry distortion. The CAMRAD II free wake geometry method gives good results for the lateral flapping at low speed. As for the airloads, the nonuniform inflow model with free wake geometry is required in order to capture the effects of strong blade-vortex interaction at low advance ratio. The CAMRAD/JA method (with baseline parameters) does not capture the lateral flapping peak. The CAMRAD/JA method with revised parameters (tip vortex core radius of 50% chord, with four revolutions of wake vorticity but the distortion calculated for only the first two revolutions) gives better results for the latter flapping at low speed, but worse results otherwise. The CAMRAD II method shows good correlation with the measured power at all speeds; the CAMRAD/JA method shows poor correlation at low speed. In particular, figure 4 shows that the induced power factor (ratio of calculated induced power to ideal momentum theory induced power) increases unrealistically at low speed with the CAMRAD/JA method.

Helicopter rotor induced power increases as the speed decreases, because of the influence of the wake geometry. Figure 5 shows the power for the S-76 rotor. Table 3 summarizes the rotor parameters and operating conditions. The wind tunnel test results are from reference 22, and the CAMRAD/JA results were discussed in reference 22. The CAMRAD II free wake geometry method shows good

correlation, while the CAMRAD/JA method overpredicts the power at low speed. Figure 6 shows the free wake geometry for the S-76, calculated by the CAMRAD II method. The change from typical forward flight behavior at $\mu = .100$ to typical hover behavior at $\mu = .025$ is observed (see also ref. 23).

The following figures illustrate the capability to calculate general free wake geometry with the CAMRAD II method. No measured data are available for correlation, but the behavior shown is reasonable. Figure 7 shows the wake geometry behind an aspect-ratio 4 nonrotating wing. The wing aerodynamic model used 25 collocation points, and the wake trailed vorticity was discretized using 13 spanwise panels. The wake geometry was calculated for each of the line-vortices at the boundaries between panels. The expected rollup of the wake at the tips is observed. This kind of rollup calculation is not useful for rotors, since it is known from both experiments and computations that the tip vortex already has a well-defined core by the time it reaches the blade trailing edge (although further entrainment of trailed vorticity occurs in the wake). Hence the rollup of rotor blade tip vortices is not an inviscid problem. The CAMRAD II capability to calculate the rollup of wakes with multiple trailed vortices is applicable to cases such as rotors with flaps or rapid chord changes, for which some significant inboard rollup is possible.

Figure 8 shows the wake geometry calculated for a wind turbine. The influence of the ground boundary layer on the wake geometry is evident. Figure 9 shows the wake geometry calculated for the XV-15 tiltrotor in helicopter mode flight. The mutual interference between the two rotors is not large for the side-by-side configuration. Figure 10 shows the wake geometry calculated for the ABC coaxial helicopter. Figure 11 shows the wake geometry calculated for the CH-46 tandem helicopter. For the coaxial and tandem configurations, the mutual interaction between the wakes of the two rotors produces wake geometry that is significantly different from that predicted for the isolated rotors.

Concluding Remarks

A general free wake geometry calculation for wings and rotors has been presented. The method gives good performance and airloads correlation at advance ratios of 0.05 and above, with reasonable computation speed. The wake geometry distortion can be calculated for multiple wings, multiple rotors, and non-identical blades; for all wake structures, including multiple rolled-up trailed vorticity and inboard sheets as well as tip vortices; using the same wake model as the induced velocity calculations;

for transients as well as the trim solution. The method has been implemented in CAMRAD II.

Additional comparisons with measured data are needed to confirm the capabilities of this general free wake geometry method. In particular, comparisons with airloads measured at low speeds are desirable, and comparisons with airloads and performance for multiple rotor configurations. Application of the method to the calculation of hovering rotor wake geometry may also be considered.

References

- 1) Johnson, W. "A Comprehensive Analytical Model of Rotorcraft Aerodynamics and Dynamics." NASA TM 81182, June 1980.
- 2) Johnson, W. "Development of a Comprehensive Analysis for Rotorcraft." *Vertica*, Volume 5, Numbers 2 and 3, 1981.
- 3) Johnson, W. "Wake Model for Helicopter Rotors in High Speed Flight." NASA CR 177507, November 1988.
- 4) Johnson, W. "Airloads and Wake Models for a Comprehensive Helicopter Analysis." *Vertica*, Volume 14, Number 3, 1990.
- 5) Johnson, W. "CAMRAD/JA, A Comprehensive Analytical Model of Rotorcraft Aerodynamics and Dynamics, Johnson Aeronautics Version." Johnson Aeronautics, Palo Alto, California, 1988.
- 6) Johnson, W. "Technology Drivers in the Development of CAMRAD II." American Helicopter Society, Aeromechanics Specialists Meeting, San Francisco, January 1994.
- 7) Johnson, W. "CAMRAD II, Comprehensive Analytical Model of Rotorcraft Aerodynamics and Dynamics." Johnson Aeronautics, Palo Alto, California, 1992, 1994.
- 8) Yen, J.G.; Corrigan, J.J.; Schillings, J.J.; and Hsieh, P.Y. "Comprehensive Analysis Methodology at Bell Helicopter: COPTER." American Helicopter Society, Aeromechanics Specialists Meeting, San Francisco, January 1994.
- 9) Yen, J.G.; Yuce, M.; Chao, C.-F., and Schillings, J. "Validation of Rotor Vibratory Airloads and Application to Helicopter Response." *Journal of the American Helicopter Society*, Volume 35, Number 4, October 1990.
- 10) Torok, M.S., and Berezin, C.R. "Aerodynamic and Wake Methodology Evaluation Using Model UH-60A Experimental Data." *Journal of the American Helicopter Society*, Volume 39, Number 2, April 1994.
- 11) Bir, G., and Chopra, I. "Status of University of Maryland Advanced Rotorcraft Code (UMARC)." American Helicopter Society, Aeromechanics Specialists Meeting, San Francisco, January 1994.
- 12) Bir, G.; Chopra, I.; et al. "University of Maryland Advanced Rotorcraft Code (UMARC), Theory Manual." UM-AERO 92-02, May 1992.
- 13) Ormiston, R.A.; Rutkowski, M.J.; Ruzicka, G.C.; Saberi, H.; and Jung, Y. "Comprehensive Aeromechanics Analysis of Complex Rotorcraft using 2GCHAS." American Helicopter Society, Aeromechanics Specialists Meeting, San Francisco, January 1994.
- 14) U.S. Army, "2GCHAS Theory Manual (Version 2.3)", USAATCOM TM 93-A-004, March 1994.
- 15) Scully, M.P. "Computation of Helicopter Rotor Wake Geometry and Its Influence on Rotor Harmonic Airloads." Massachusetts Institute of Technology, ASRL TR 178-1, March 1975.
- 16) Landgrebe, A.J. "An Analytical Method for Predicting Rotor Wake Geometry." *Journal of the American Helicopter Society*, Volume 14, Number 4, October 1969.
- 17) Bliss, D.B.; Teske, M.E.; and Quackenbush, T.R. "A New Methodology for Free Wake Analysis Using Curved Vortex Elements." NASA CR 3958, December 1987.
- 18) Scheiman, J., and Ludi, L.H. "Qualitative Evaluation of Effect of Helicopter Rotor-Blade Tip Vortex on Blade Airloads." NASA TN D-1637, May 1963.
- 19) Heffernan, R.M., and Gaubert, M. "Structural and Aerodynamic Loads and Performance Measurements of an SA349/2 Helicopter with an Advanced Geometry Rotor." NASA TM 88370, November 1986.
- 20) Johnson, W. "Calculation of Blade-Vortex Interaction Airloads on Helicopter Rotors." *Journal of Aircraft*, Volume 26, Number 5, May 1989.
- 21) Harris, F.D. "Articulated Rotor Blade Flapping Motion at Low Advance Ratio." *Journal of the American Helicopter Society*, Volume 17, Number 1, January 1972.
- 22) Shinoda, P., and Johnson, W. "Performance Results from a Test of an S-76 Rotor in the NASA Ames 80- by 120-Foot Wind Tunnel." AIAA Paper Number 93-3414, August 1993.
- 23) Miller, W.O., and Bliss, D.B. "Direct Periodic Solutions of Rotor Free Wake Calculations." *Journal of the American Helicopter Society*, Volume 38, Number 2, April 1993.

analysis (references)	wake model	wake geometry model
CAMRAD (1,2)	single peak circulation; first order lifting line theory	Scully
CAMRAD mod (3,4) COPTER (8,9) RDYNE (10) UMARC (11,12) 2GCHAS (13,14)	single/dual peak circulation; second order lifting line theory	Scully
CAMRAD/JA (5)	" "	Scully
CAMRAD/JA mod	" "	Scully, Johnson
CAMRAD II (6,7)	single/dual peak circulation; second order lifting line theory; entrainment and stretching model for rollup process; multiple rollup of trailede wake	Scully, Johnson, general

Table 1. Wake geometry and wake models in rotorcraft analyses.

	performance	baseline	low speed
wake distortion required τ_{\max} (revs)	.4/ μ	.4/ μ	.4/ μ
number of azimuth steps J (per rev)	24	24	24
young wake extent τ_{young} (revs)	1/ N	1/ N	2/ N
far wake update frequency n_F (revs)			
young	1/2	1/ J	1/ J
elder	1/2	1/2	1/2
near wake update frequency n_N (revs)			
young	1/8	1/ J	1/ J
elder	1/8	1/8	1/8
near wake velocity criterion	0.0005 V	0.0005 V	0.0003 V
bound vortex velocity criterion	0.0005 V	0.0005 V	0.0003 V
velocity relaxation factor λ_R	0.5	0.5	0.2
integration time MT	2 or 3 τ_{\max}	2 or 3 τ_{\max}	2 or 3 τ_{\max}
M_{below} (revs)	2	2	4

Table 2. Parameters of wake geometry calculation (N = number of wings; V = tip speed).

	H-34	SA349/2	Model	S-76
Number of blades	4	3	4	4
Radius, ft	28.00	17.22	2.73	22.00
Solidity ratio	0.062	0.064	0.089	0.0748
Airfoil	NACA0012	OA209	V23010-1.58	SC1095 SC1095R8
C_T/σ	0.087	0.065	0.080	0.065–0.100
μ	0.18	0.14	0–0.24	0–0.25
Advancing tip Mach number	0.70	0.72	0.40–0.50	0.605–0.756
Reference	18	19	21	22

Table 3. Rotor parameters and operating conditions for comparisons with measured data.

number of blades	2	4	6
number of wake revs	2	3	4
number of azimuth steps	24	24	24
CAMRAD/JA	1.3	5.4	13.7
CAMRAD II	6.9	21.8	64.0
CAMRAD II, performance	2.9	14.0	41.9
CAMRAD II, baseline	6.9	21.8	64.0
CAMRAD II, low speed	17.8	43.0	96.1

Table 4. Computation times of wake geometry models (seconds on DEC 3000 AXP 400).

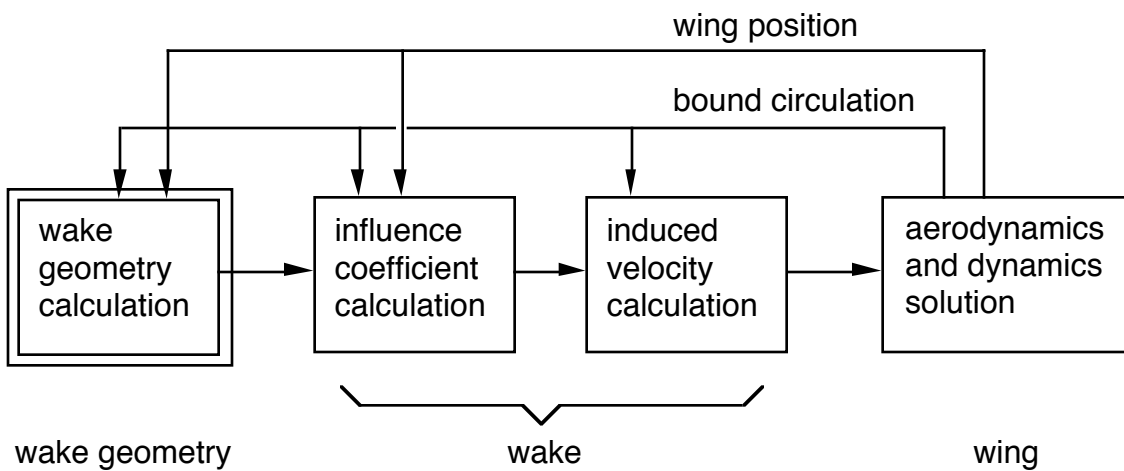


Figure 1. Rotor aerodynamics calculations.

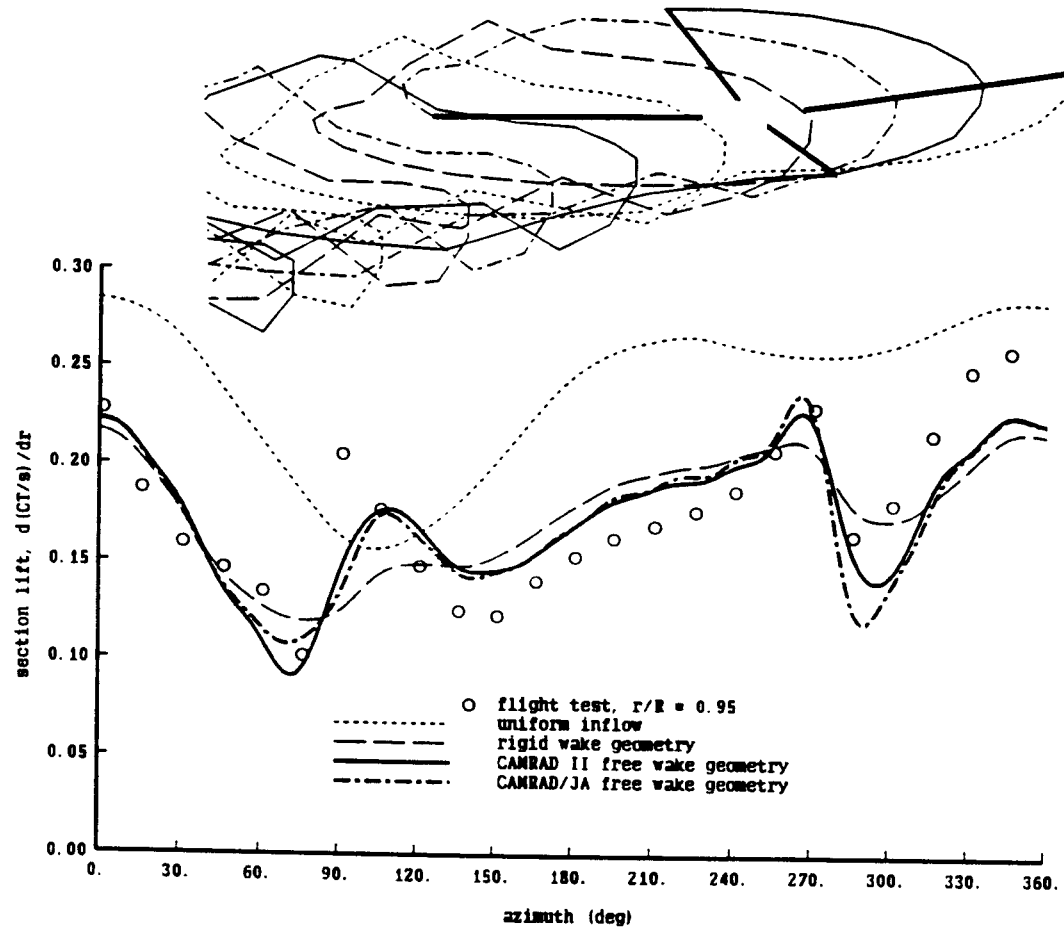


Figure 2. H-34 flight test; $C_T/\sigma = .087$, $\mu = .18$.

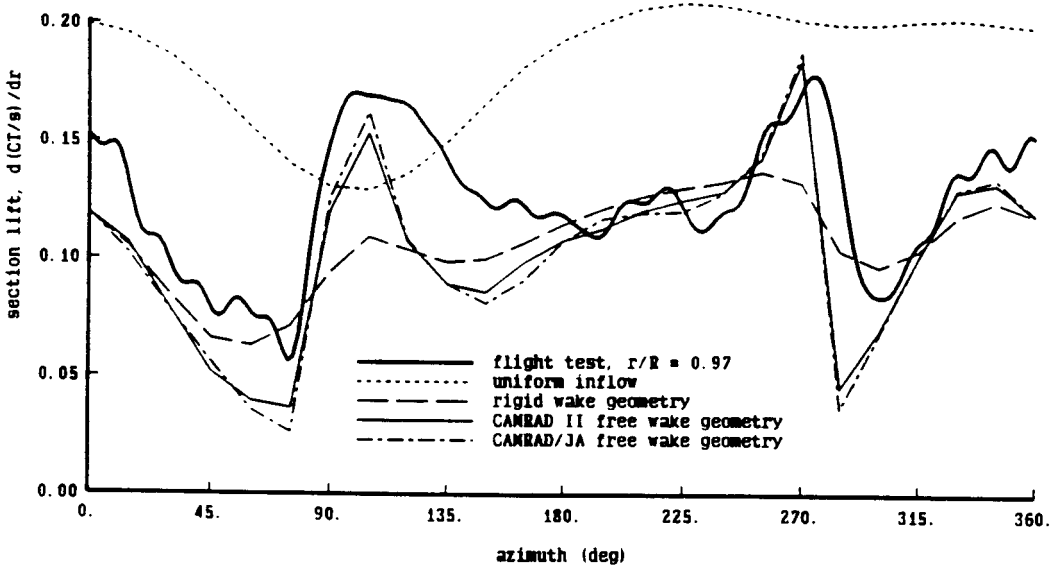


Figure 3. SA-349/2 flight test; $C_T/\sigma = .065$, $\mu = .14$.

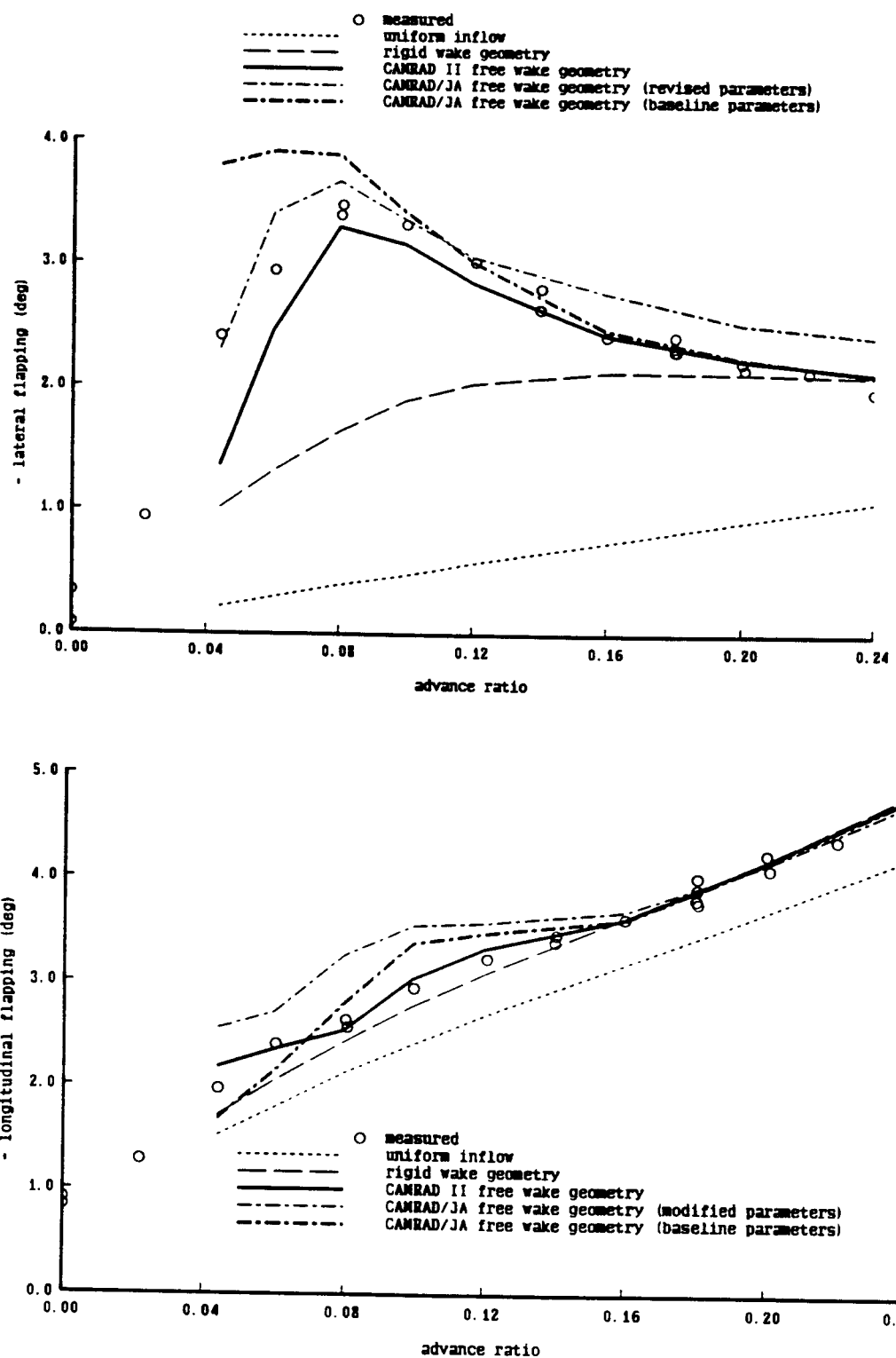


Figure 4a. Model rotor test; $C_T/\sigma = .08$, $\alpha_{tpp} \approx 1$ deg.

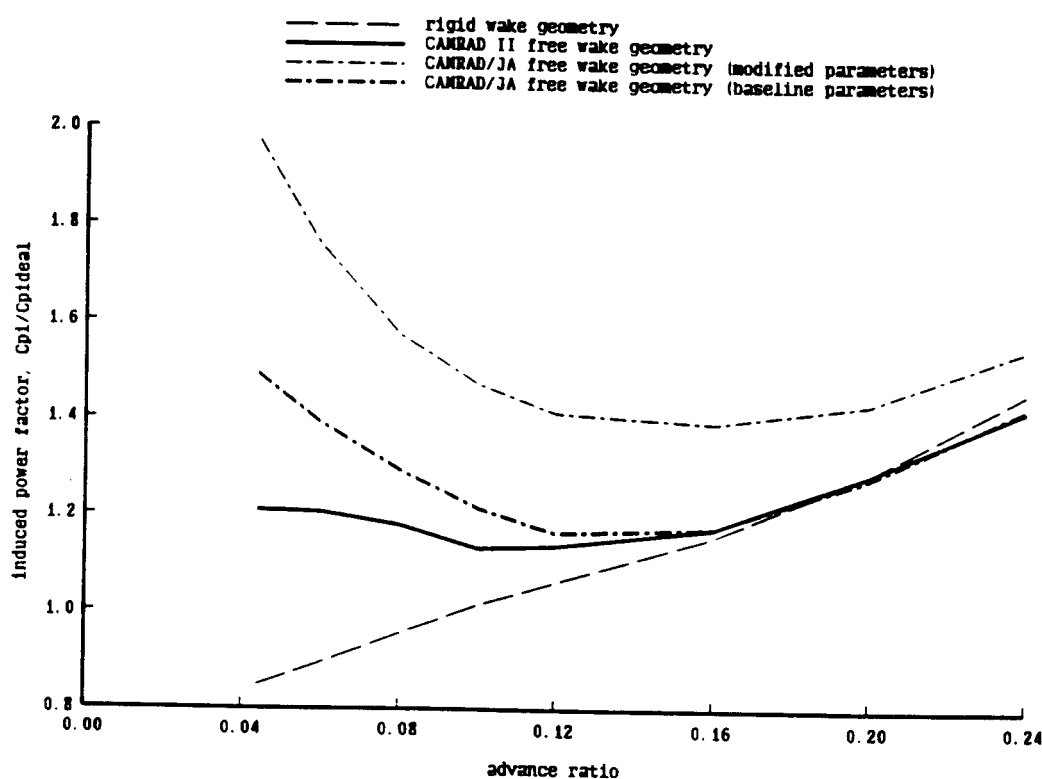
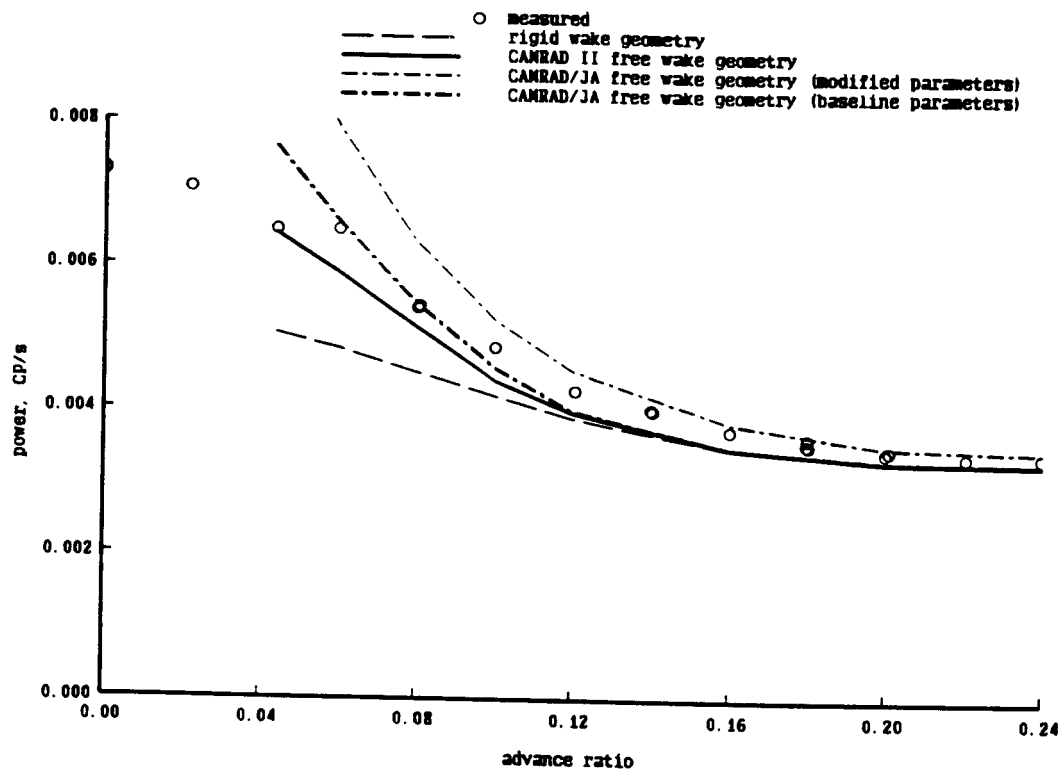


Figure 4b. Model rotor test; $C_T/\sigma = .08$, $\alpha_{tpp} \approx 1$ deg.

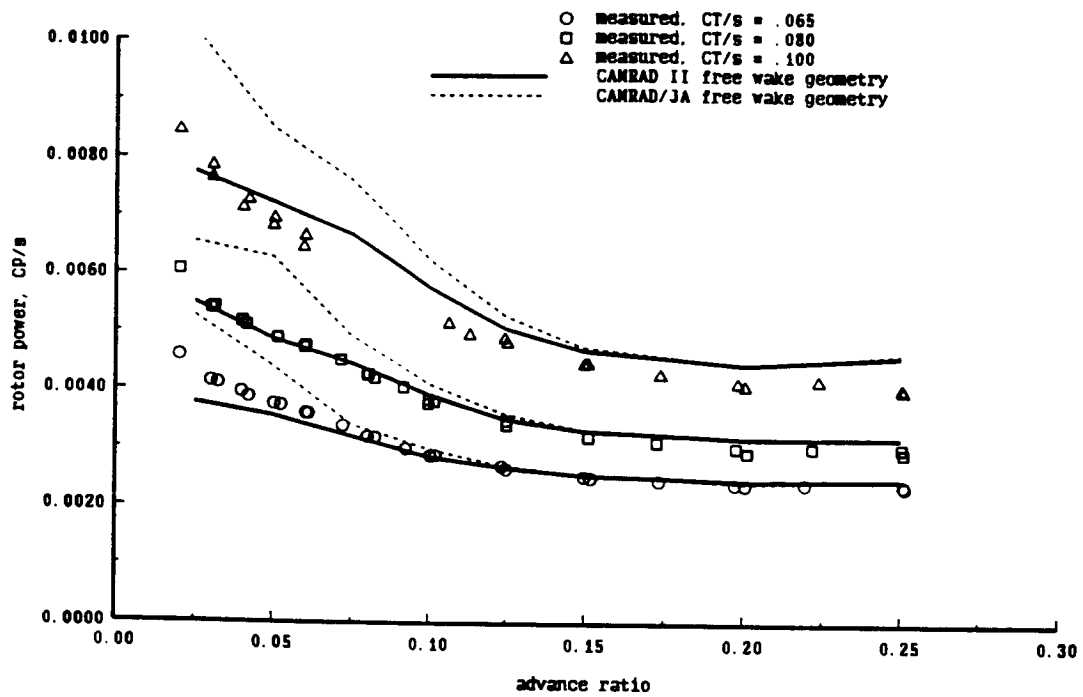


Figure 5. S-76 wind tunnel test; $\alpha_s = -2$ deg.



Figure 6. S-76 free wake geometry; $CT/\sigma = .08$, $\alpha_s = -2$ deg, $\mu = .025$ to $.100$.

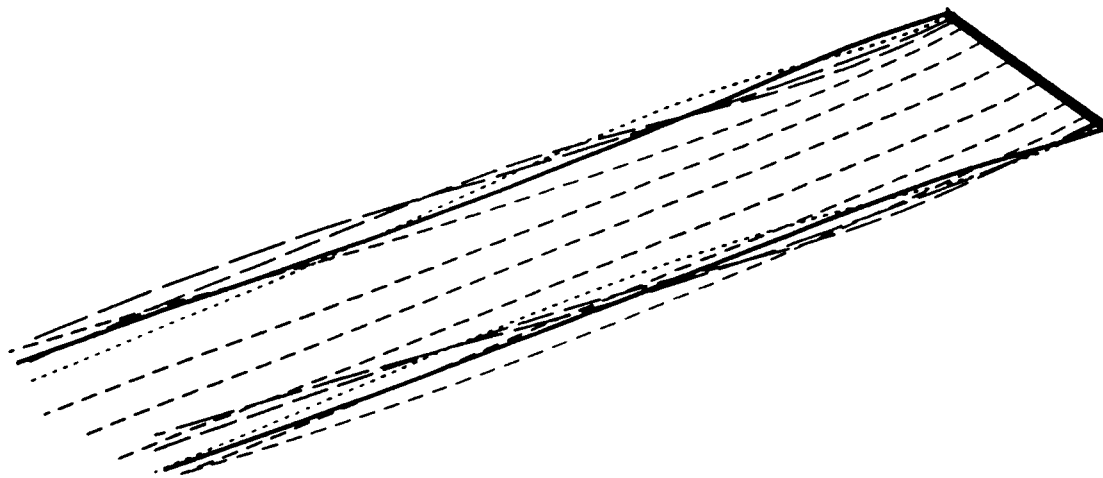


Figure 7. Calculated free wake geometry of nonrotating wing.

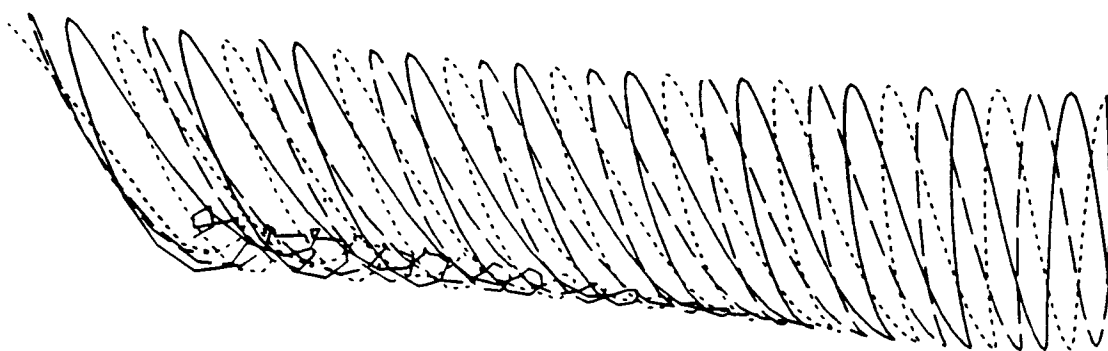


Figure 8. Calculated free wake geometry of wind turbine; power = 1.3MW, $\Omega R/V = 6.8$ ($C_T/\sigma = .08$, $\mu = .15$).

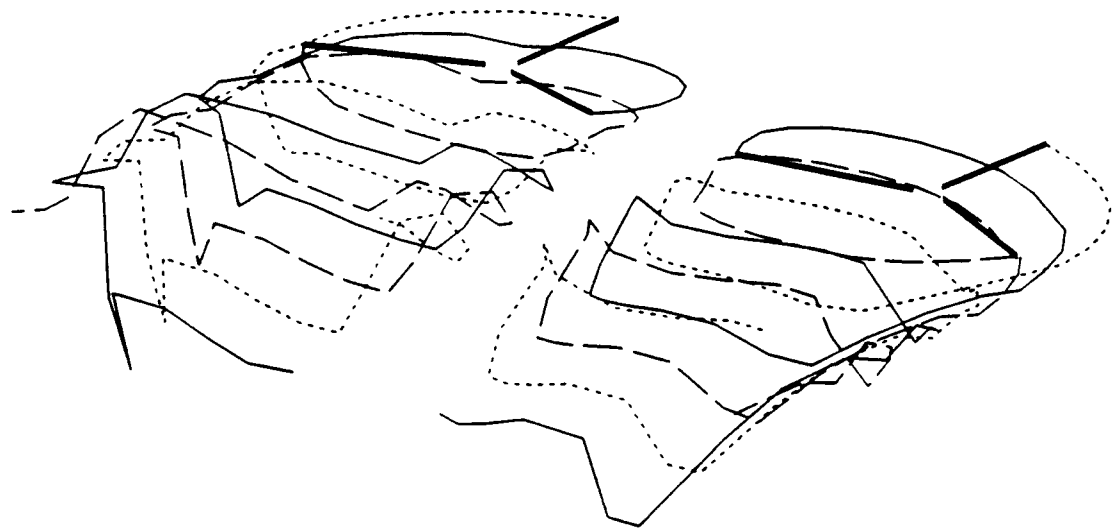


Figure 9. Calculated free wake geometry of XV-15 tiltrotor in helicopter mode flight; $C_T/\sigma = .084$, $\mu = .18$.

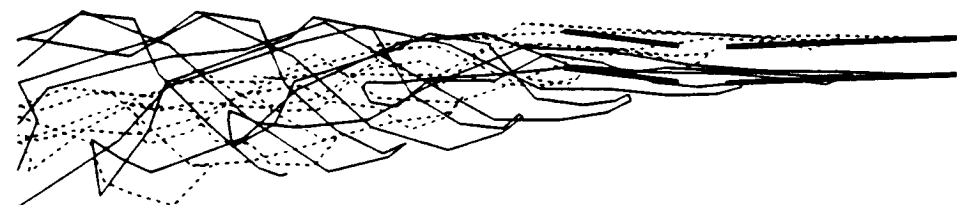
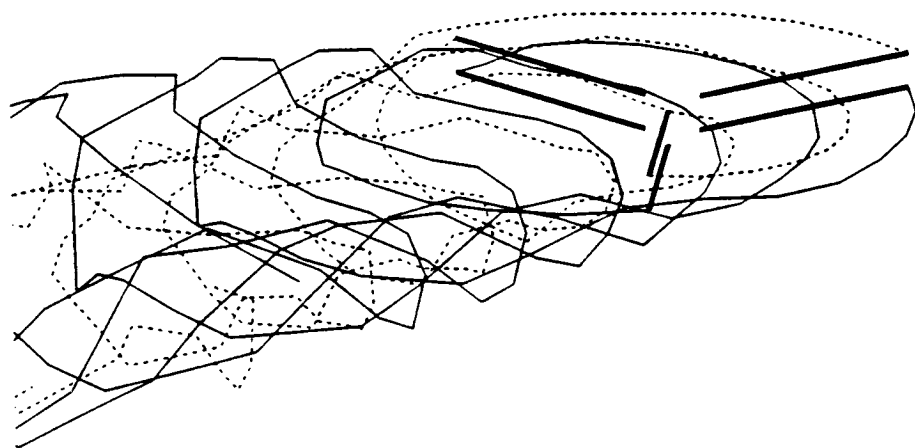


Figure 10a. Calculated free wake geometry of ABC coaxial helicopter; $C_T/\sigma = .104$, $\mu = .21$.

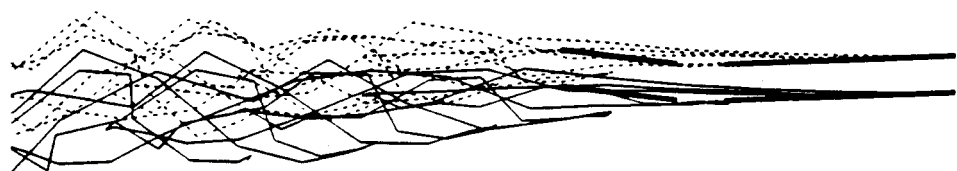


Figure 10b. Calculated free wake geometry of ABC coaxial helicopter; isolated rotor wake geometry.

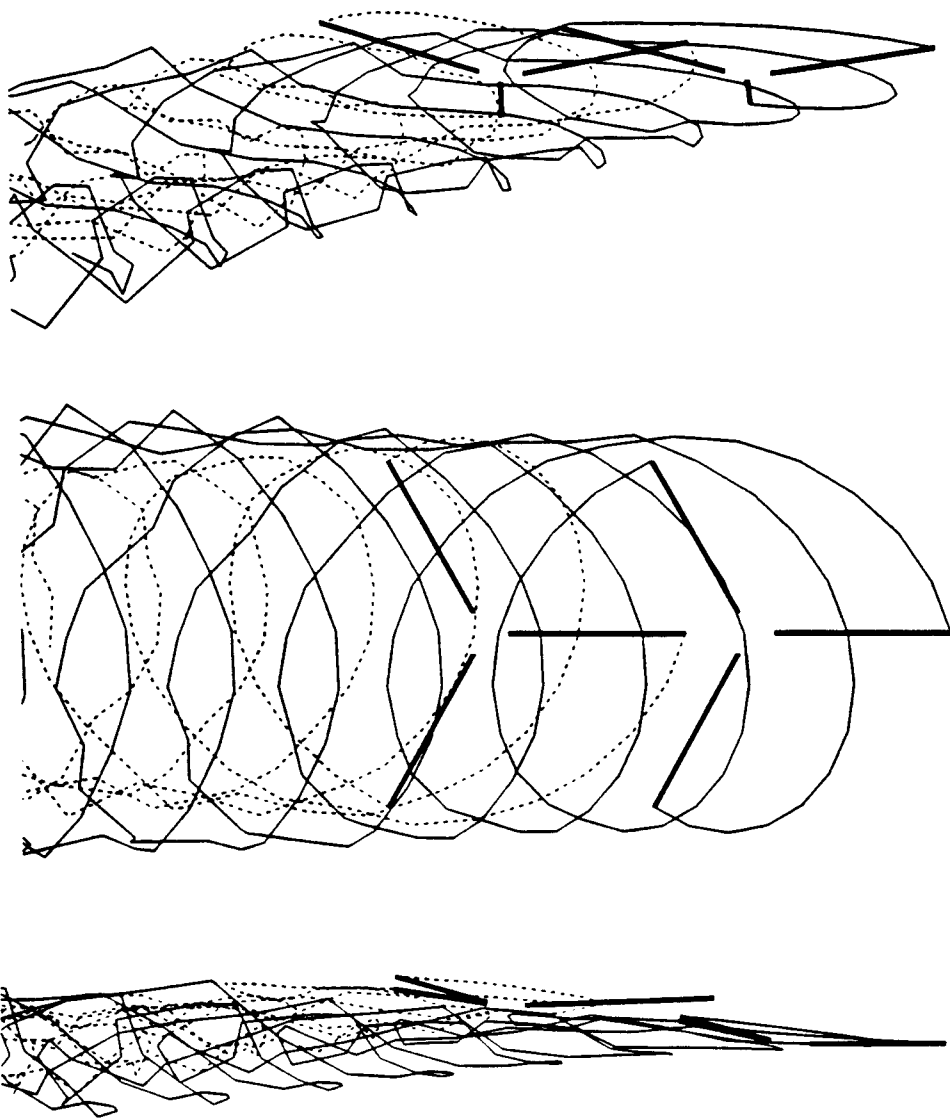


Figure 11a. Calculated free wake geometry of CH-46 tandem helicopter; $C_T/\sigma = .075$, $\mu = .24$.

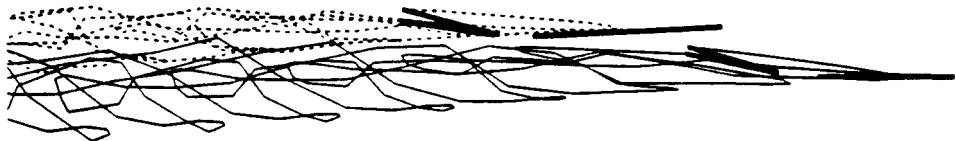


Figure 11b. Calculated free wake geometry of CH-46 tandem helicopter; isolated rotor wake geometry.